PNAS RESEARCH ARTICLE | PHYSIOLOGY OPEN ACCESS

Postprandial cardiac hypertrophy is sustained by mechanics, epigenetic, and metabolic reprogramming in pythons

Claudia Crocini[a,b,c], Kathleen C. Woulfe[d], Christopher D. Ozeroff[b,c], Stefano Perni[e], Joseph Cardiello[b], Cierra J. Walker[b], Cortney E. Wilson[d], Kristi Anseth[b], Mary Ann Allen[b], and Leslie A. Leinwand[b,c,1]

Affiliations are included on p. 8.

Edited by Jeffery D. Molkentin, Cincinnati Children's Hospital Medical Center, Cincinnati, OH; received January 17, 2024; accepted June 18, 2024 by Editorial Board Member Andrew R. Marks

Constricting pythons, known for their ability to consume infrequent, massive meals, exhibit rapid and reversible cardiac hypertrophy following feeding. Our primary goal was to investigate how python hearts achieve this adaptive response after feeding. Isolated myofibrils increased force after feeding without changes in sarcomere ultrastructure and without increasing energy cost. Ca^{2+} transients were prolonged after feeding with no changes in myofibril Ca^{2+} sensitivity. Feeding reduced titin-based tension, resulting in decreased cardiac tissue stiffness. Feeding also reduced the activity of sirtuins, a metabolically linked class of histone deacetylases, and increased chromatin accessibility. Transcription factor enrichment analysis on transposase-accessible chromatin with sequencing revealed the prominent role of transcription factors Yin Yang1 and NRF1 in postfeeding cardiac adaptation. Gene expression also changed with the enrichment of translation and metabolism. Finally, metabolomics analysis and adenosine triphosphate production demonstrated that cardiac adaptation after feeding not only increased energy demand but also energy production. These findings have broad implications for our understanding of cardiac adaptation across species and hold promise for the development of innovative approaches to address cardiovascular diseases.

cardiac mechanics | heart hypertrophy | titin | epigenetic | metabolism

Significance

Constricting pythons increase cardiac mass and output after consumption of a meal. This study explores python cardiac adaptation in the first 24 h after feeding, identifying a remarkably fast orchestration of this response. Python hearts increased myofibril contraction force at no energy cost, prolonged Ca^{2+} transients, and reduced titin-based cardiac tension to support cardiac output and improve cardiac filling. Changes in histone-deacetylase activity, transcription factor accessibility, and gene expression contributed to enhance protein synthesis and folding. Metabolic reprogramming increased adenosine triphosphate production via oxidative phosphorylation. Our work demonstrates the fine-tuned coordination of key elements of python cardiac biology and may inform our understanding of cardiac adaptation in other species and human cardiovascular diseases.

Animals residing in extreme environments have developed unique survival mechanisms, offering valuable insights for potential applications in human health. One such group of animals is constricting pythons that eat very large infrequent meals (1). This extreme physiological metabolic regulation requires the coordination of multiple organ systems, including the cardiovascular system. After feeding, pythons double their heart rate (2) and show increased oxygen consumption (3, 4), increased cardiac output (5–8), and cardiac hypertrophy (1, 9, 10). Previous work has linked postprandial cardiac adaptation to a reduction of parasympathetic tone (11) and to factors circulating in the python plasma, such as nonadrenergic, noncholinergic factors (2, 11, 12) and fatty acids (10). The increased cardiac output has been attributed largely to increased heart rate and cardiac filling rather than changes in contractility per se (7, 8), but isolated cardiac myofibrils have not yet been studied. Changes occurring in python myofibrils after feeding may underlie the improved cardiac filling observed after feeding. Despite an earlier report of a single python cardiac myosin heavy chain (13), we have found that python hearts coexpress several myosin heavy chains including three that are not expressed in mammalian hearts (14). Previous work demonstrated increased messenger RNA of ventricular myosin heavy chain (9), but there have been no reports of how feeding affects myosin isoform expression or function. Conclusions from studies thus far point to python cardiac adaptation after feeding as beneficial or physiological hypertrophy with significantly higher activities of cytochrome oxidase and pyruvate kinase (7), increased activation of PI3K/Akt/mTor signaling pathways (10), and increased activity and expression of the cardioprotective SOD2. Previous studies in Burmese pythons have also reported gene expression changes related to metabolism (13, 15, 16), but the cardiac metabolome has not yet been investigated.

Many questions remain about the postprandial response of the python heart. We focused here on early responses to feeding and compared fasted ball python hearts to those 24 h postfeeding. We used a combination of approaches, in an effort to correlate functional observations with changes in structure, molecular signaling, gene expression, and epigenetics. Our findings indicate that feeding changed myofibril active and passive forces as well as modified chromatin accessibility, likely to promote a gene expression program that sustains translation and metabolism. In summary, our study provides insights into the molecular mechanisms

The authors declare no competing interest.

This article is a PNAS Direct Submission. J.D.M. is a guest editor invited by the Editorial Board.

[1]To whom correspondence may be addressed. Email: leslie.leinwand@colorado.edu.

This article contains supporting information online at https://www.pnas.org/lookup/suppl/doi:10.1073/pnas.2322726121/-/DCSupplemental.

Published August 19, 2024.

Table 1. Gene names and accession numbers used for protein identification in mass spectrometry

Gene	Accession number
pyMYH1	XP_025018919.1
pyMYH3	XP_025018918.1
pyMYH6	XP_025029596.1
pyMYH7	XP_025029595.1
pyMYH7b	XP_007419944.1
pyMYH15	XP_007429332.1
pyMYH16	XP_025026462.1

underlying python cardiac biology and may have important implications for understanding cardiac adaptation in other species and for developing novel therapies for cardiovascular diseases.

Results

Isolated Myofibrils of Ball Python Hearts Generate Greater Force after Feeding. To investigate early changes in cardiac muscle function after feeding, we employed fasted (28 d) and 24 h postfed pythons (fed a meal 25% of their body mass Fig. 1*A*). Similar to Burmese pythons (3, 10), ball python hearts increased 24.5% in mass 24 h after feeding compared to fasted hearts (Fig. 1*B* and *SI Appendix*, Fig. S1*A*). Electron microscopy confirmed increased size of muscle fibers after feeding (Fig. 1 *C* and *D*) but at this timepoint, it did not appear to be the result of increased myofibril content (Fig. 1*E*). Sarcomere and A-band lengths were not different between fasted and 24 h postfed pythons (Fig. 1 *F*–*H*). In the absence of ultrastructural changes, we hypothesized that the function of cardiac myofibrils would change in response to feeding. Isolated single myofibrils of 24 h postfed pythons generated more force than myofibrils from fasted pythons (Fig. 1*I*) with no differences in the activation rates (kact and ktr) (*SI Appendix*, Fig. S1*B* and Fig. 1*J*, respectively). Relaxation time of 24 h postfed myofibrils was prolonged as compared to fasted myofibrils (Fig. 1*K*), most likely as a result of a slower linear phase of the relaxation rate (krel, lin) with no change in the exponential phase of relaxation (krel, exp; Fig. 1*L* and *SI Appendix*, Fig. S1*C*). As previously shown (14), pythons hearts coexpress several myosin isoforms (*SI Appendix*, Fig. S1*D*). Mass spectrometry indicated that both fasted and 24 h postfed hearts expressed the different myosin isoforms similarly, with MYH15 being the most abundant myosin, followed by MYH7B, MYH6, MYH7, MYH1, and MYH3 (Table 1). Fasted hearts also expressed MYH16 at very low levels (~2% of all myosins) compared to the other isoforms, but it was not detected in 24 h postfed python hearts (*SI Appendix*, Table S1). Only Ser309 of the cardiac myosin binding protein-C (cMyBP-C) was phosphorylated (Best Ascore 1,000 and localization probability 100%) in both fasted and 24 h postfed (*SI Appendix*, Table S2). This result was confirmed by Pro-Q Diamond staining (*SI Appendix*, Fig. S1*E*).

Prolonged Ca^{2+} Transients after Feeding Are Not Associated with Changes in Myofibril Ca^{2+} Sensitivity. Next, we investigated the effect of feeding on Ca^{2+} transients in isolated python cardiomyocytes (*SI Appendix*, Fig. S2*A*). Cardiomyocytes from 24 h postfed hearts showed significantly prolonged Ca^{2+} transients both at Ca^{2+} rise (time-to-peak) and Ca^{2+} decay at 50% (Fig. 2 *A* and *B*). We tested whether changes in myofibril Ca^{2+} sensitivity could account for the prolonged Ca^{2+} transients. However, Ca^{2+} sensitivity of myofibrils did not change after feeding (Fig. 2*C*), as also confirmed by the unchanged phosphorylation of cardiac troponin I (cTnI), the main target for altering myofibril Ca^{2+} sensitivity in cardiomyocytes (*SI Appendix*, Fig. S2*B*). We then measured python peripheral couplings, Ca^{2+}-containing-structures that run parallel to the surface membrane that represent the entirety of the sarcoplasmic reticulum in reptiles (17). Peripheral coupling length was increased in 24 h postfed cardiomyocytes as compared to fasted (Fig. 2*D*), possibly to maintain Ca^{2+} amplitude. Considering the increased fiber size, we posit that prolongation of Ca^{2+} transients could be due to the increased cellular volume. From the EM images, we measured the space that was not occupied by myofilaments and found increased intermyofibrillar space in 24 h postfed cardiomyocytes as compared to fasted (Fig. 2*E*).

Myofibril Passive Tension and Cardiac Tissue Stiffness Were Reduced after Feeding. Isolated myofibrils from 24 h postfed python hearts showed lower resting tension as a function of sarcomere length than fasted myofibrils (Fig. 3*A* and *SI Appendix*, Fig. S3*A*). In general, python myofibrils showed a remarkable compliance and could be stretched more than mammalian cardiac myofibrils (18). Within myofibrils, titin is the main source of passive tension (18) and, in mammals, it can be expressed in different isoforms with varying compliance via alternative splicing (19). Titin protein gels suggested that only one titin isoform was expressed in fasted and 24 h postfed hearts (Fig. 3*B*), and it was longer than mammalian titin cardiac isoforms (Fig. 3*B*). The isoform is predicted to be 3,621 kDa (XP_025018685.1) and included the N2B cardiac region and a serine and a cysteine that are conserved in human, mice, and chicken (20) (annotated sequence provided in *SI Appendix*). We hypothesized that the reduced myofibril passive tension would be sufficient to affect bulk cardiac tissue stiffness. Using a rheometer, we found that 24 h postfed ventricle tissue was significantly less stiff than fasted hearts (Fig. 3*C*) and that overall python tissue stiffness is about five times less than that of mouse ventricles (*SI Appendix*, Fig. S3*B*, mouse data previously published in ref. 21).

Postprandial Epigenetic Modifications Regulate Transcription and Translation. Based on the very rapid and robust responses of the 24 h postfed python heart, we tested the hypothesis that epigenetic modifications likely contribute to these functional changes. We measured the open and closed states of chromatin in both fasted and fed states in isolated python cardiomyocytes. Using confocal imaging, we calculated the chromatin condensation parameter (CCP) of isolated cardiomyocytes identified by the expression of myosin (*SI Appendix*, Fig. S2*A*). Cardiomyocytes from 24 h postfed hearts showed significantly reduced chromatin condensation compared to fasted hearts (Fig. 4*A*). Consistently, histone-3 acetylation was increased in 24 h postfed hearts as compared to fasted (Fig. 4*B*). We then measured the activity of histone deacetylases (HDACs), a family of epigenetic regulatory enzymes that control chromatin accessibility through deacetylation of nucleosomal tails. Total HDAC activity was not significantly different between fasted and 24 h postfed hearts (Fig. 4*C*). We then treated lysates with trichostatin A (TSA), a well-known inhibitor of Class I and Class II HDACs (22) but not Class III HDACs, also called sirtuins. After TSA, the residual HDAC activity was significantly lower in 24 h postfed hearts as compared to fasted (Fig. 4*D*). This result demonstrated that feeding specifically reduced the activity of sirtuins in python hearts. We next performed the assay for transposase-accessible chromatin with sequencing (ATAC-Seq), to investigate chromatin accessibility across the genome at higher

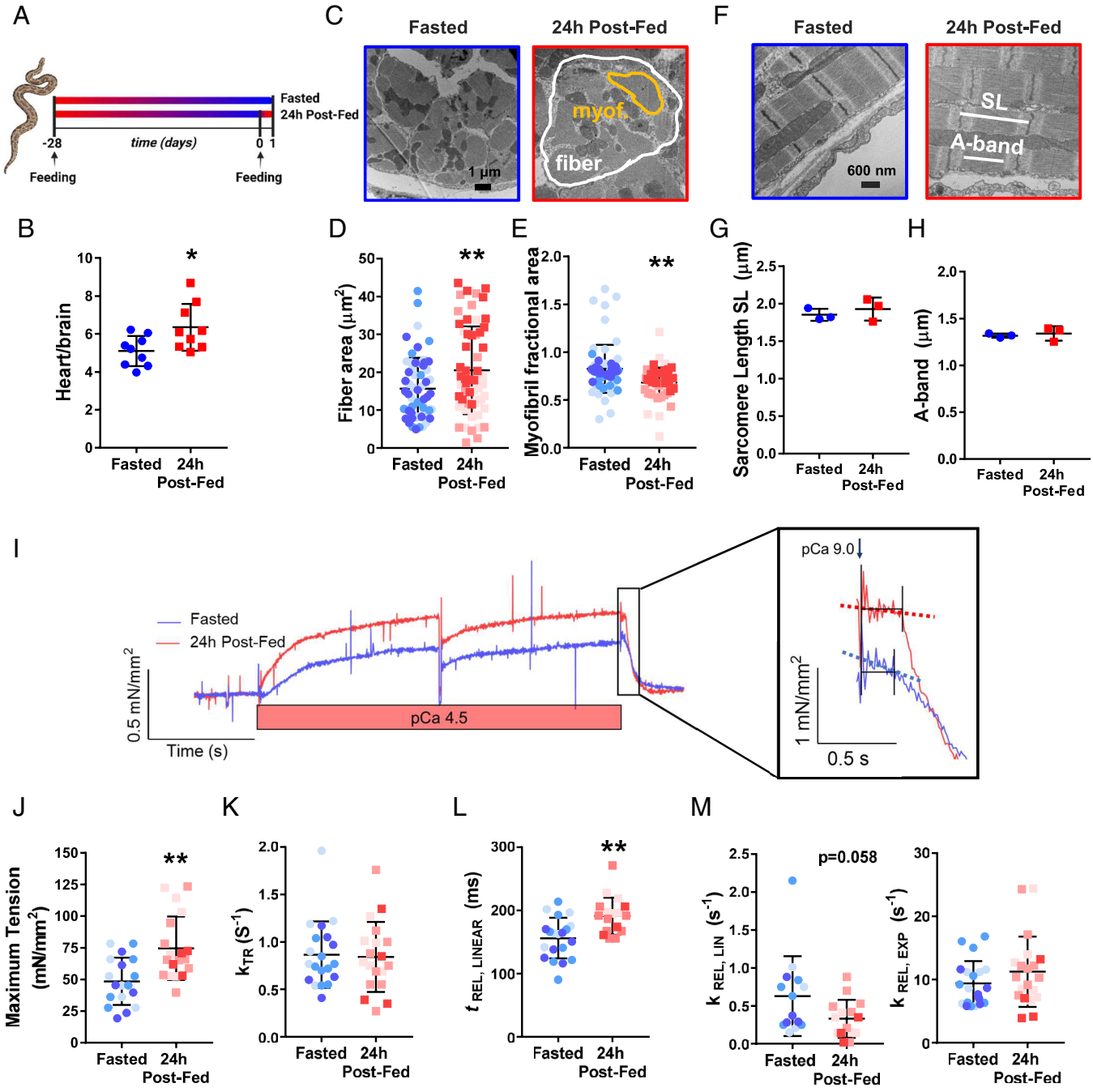

Fig. 1. Sarcomere ultrastructure was unchanged after feeding but isolated myofibrils generated greater force. (*A*) Schematic of the experimental setup. Python snakes were fasted for 28 d and fed ~25% of their body weight 24 h prior experiments. (*B*) Heart mass normalized by brain mass. Data from 9 fasted and 9 24 h postfed pythons. Student *t* test applied. (*C*) Cross-section electron microscopy images of fasted (blue) and 24 h postfed (red) hearts. Fibers and myofibrils were traced manually to measure relative sizes. (*D*) Fiber area in μm^2. N = 3 hearts per group, n = 60 fasted, and n = 59 24 h postfed fibers. Each color represents a python. Student *t* test applied. (*E*) Myofibril fractional area normalized by fiber area. N = 3 hearts per group, n = 62 fasted and n = 56 24 h postfed myofibers. Each color represents a python. Student *t* test applied. (*F*) Electron microscopy images of transversal sections of fasted (blue) and 24 h postfed (red) hearts. Sarcomere length (SL) and A-band length were measured. (*G*) Sarcomere length in fasted (blue) and 24 h postfed (red) python hearts. N = 3. Student *t* test applied. (*H*) A-band length in fasted (blue) and 24 h postfed (red) python hearts. N = 3. Student *t* test applied. (*I*) Representative mechanics traces from fasted (blue) and 24 h postfed (red) myofibrils. On the *Right*, magnification of the relaxation phase after switching from pCa 4.5 to pCa 9.0. (*J*) Maximum tension in mN/mm^2 measured in fasted (blue) and 24 h postfed (red) myofibrils. N = 3 hearts per group. n = 18 fasted and n = 19 24 h postfed myofibrils. Each color represents a python. Student *t* test applied. (*K*) Myofibril linear relaxation time in ms of fasted (blue) and 24 h postfed heart (red). N = 3 hearts per group, n = 20 fasted and n = 18 24 h postfed myofibrils. Each color represents a python. Student *t* test applied. (*L*) Resting tension as a function of sarcomere stretch. Nonlinear exponential growth fit applied. Global fits compared for kinetic parameter (k). (*M*) Bulk shear tension measured in fasted (blue) and 24 h postfed (red) hearts with a rheometer. Data reported as Young's modulus in kPa. N = 3. Student *t* test applied.

resolution (23). Transcription factor enrichment analysis on ATAC-seq data of isolated cardiomyocytes from fasted and 24 h postfed pythons identified higher accessibility of the binding site for Yin Yang1 (YY1) (corrected *P*-adj value $1e^{-5}$), a ubiquitously expressed transcriptional factor, and the nuclear factor erythroid 2-related factor 1 (NRF1, corrected *P*-adj value $1e^{-7}$), an ER-bound transcription factor member of the vertebrate Cap`n'Collar (CNC) transcription factor family (Fig. 4*E*). To identify feeding-specific gene expression signatures, we next performed RNA-sequencing (RNA-seq) on

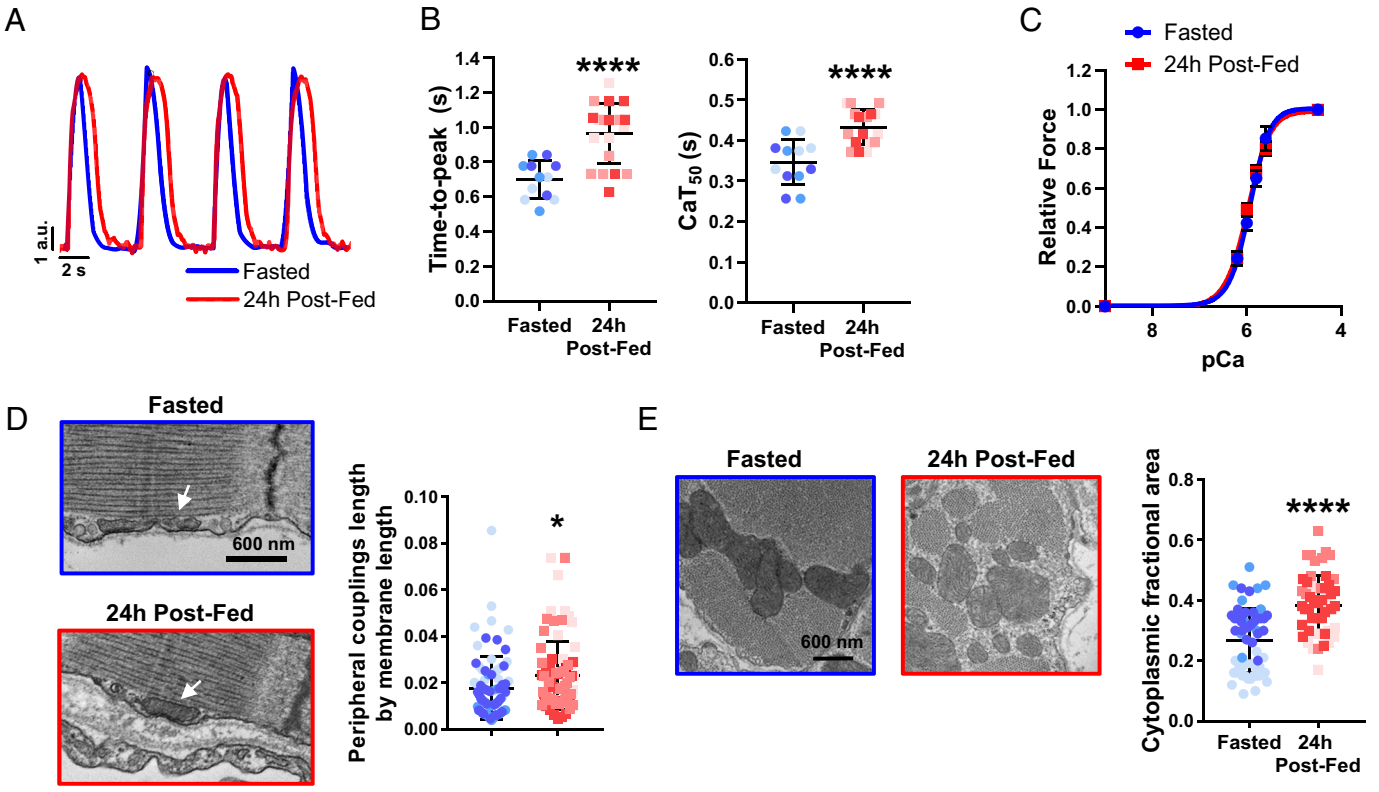

Fig. 2. Feeding-induced prolonged Ca^{2+} transients with no change in myofibril Ca^{2+} sensitivity. (*A*) Example of Ca^{2+} transients measured in fasted (blue) and 24 h postfed (red) python cardiomyocytes, stimulated at 0.2 Hz. (*B*) Averages of Ca^{2+} time-to-peak and Ca^{2+} decay at 50% (CaT_{50}). Average of 12 fasted cardiomyocytes and 20 24 h postfed cardiomyocytes. N = 3 hearts. (*C*) Ca^{2+} sensitivity curve of myofibrils from fasted (blue) and 24 h postfed (red) hearts. Average of 16 fasted myofibrils and 15 24 h postfed myofibrils. N = 3 hearts. (*D*) Electron microscopy images of longitudinal sections of fasted (blue) and 24 h postfed (red) hearts, showing peripheral couplings (white arrows). (*E*) Electron microscopy images of transversal sections of fasted (blue) and 24 h postfed (red) hearts. Cytoplasmic space quantified on the *Right*. N = 3 hearts per group, n = 62 fasted and n = 56.

fasted and 24 h postfed ventricles (24). Then, 840 genes were differentially expressed between fasted and 24 h postfed hearts (*SI Appendix*, Table S3) and gene ontology cellular component (GOCC) and biological process (GOBP) enrichment analysis identified increased involvement of the endoplasmic reticulum, increased protein folding, decreased euchromatin, and decreased histone deacetylase complex in 24 h postfed python hearts as compared to fasted (Fig. 4*F* and *SI Appendix*, Fig. S5). Then, 226 and 77 genes that were differentially expressed between fasted and 24 h postfed hearts were known targets of YY1 and NRF1, respectively (*SI Appendix*, Table S4).

Feeding Changes Metabolism to Meet Cardiac Energy Demands. Metabolism in pythons plays an important role after feeding as indicated by liver adaptation to plasma hyperlipidemia (25) and fatty-acid-induced cardiac hypertrophy (10). Notably, sirtuins, YY1, and NRF1 have all been linked to metabolism. Sirtuins are activated by an NAD^+ increase during caloric restriction (26). YY1 has been shown to up-regulate pathways related to the tricarboxylic acid cycle, respiratory electron transport, and adenosine triphosphate (ATP) synthesis (27), and NRF1 has been recently shown to confer cardioprotection in the adult heart via redox balancing (28). Given the substantially high enrichment of

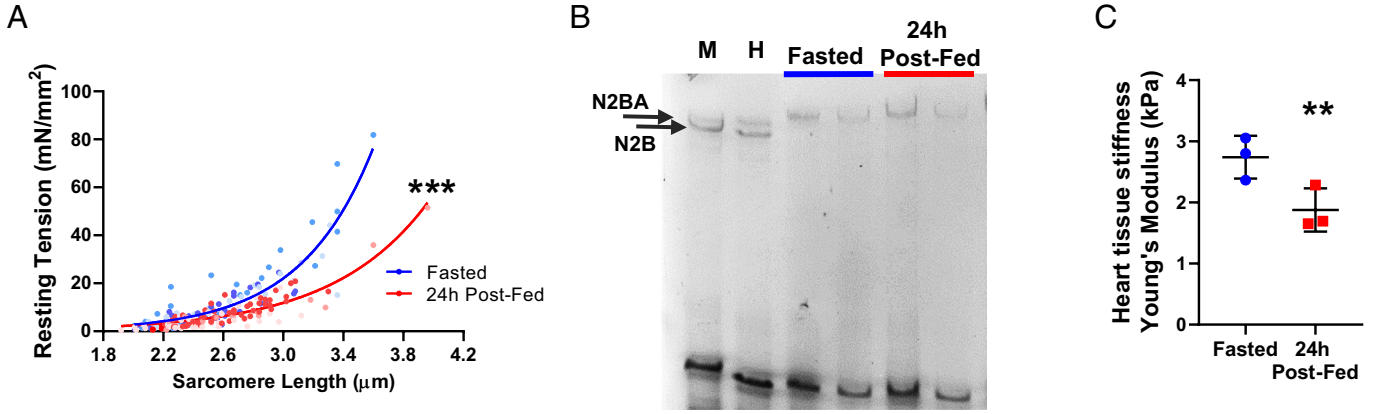

Fig. 3. Feeding reduced myofibril passive tension and tissue stiffness. (*A*) Resting tension as a function of sarcomere stretch. Nonlinear exponential growth fit applied. Global fits compared for kinetic parameter (k). (*B*) Titin gel of fasted (blue) and 24 h postfed (red) heart tissue. Mouse (M) and Human (H) heart tissues as reference. (*C*) Bulk shear tension measured in fasted (blue) and 24 h postfed (red) hearts with a rheometer. Data reported as Young's modulus in kPa. N = 3. Student *t* test applied.

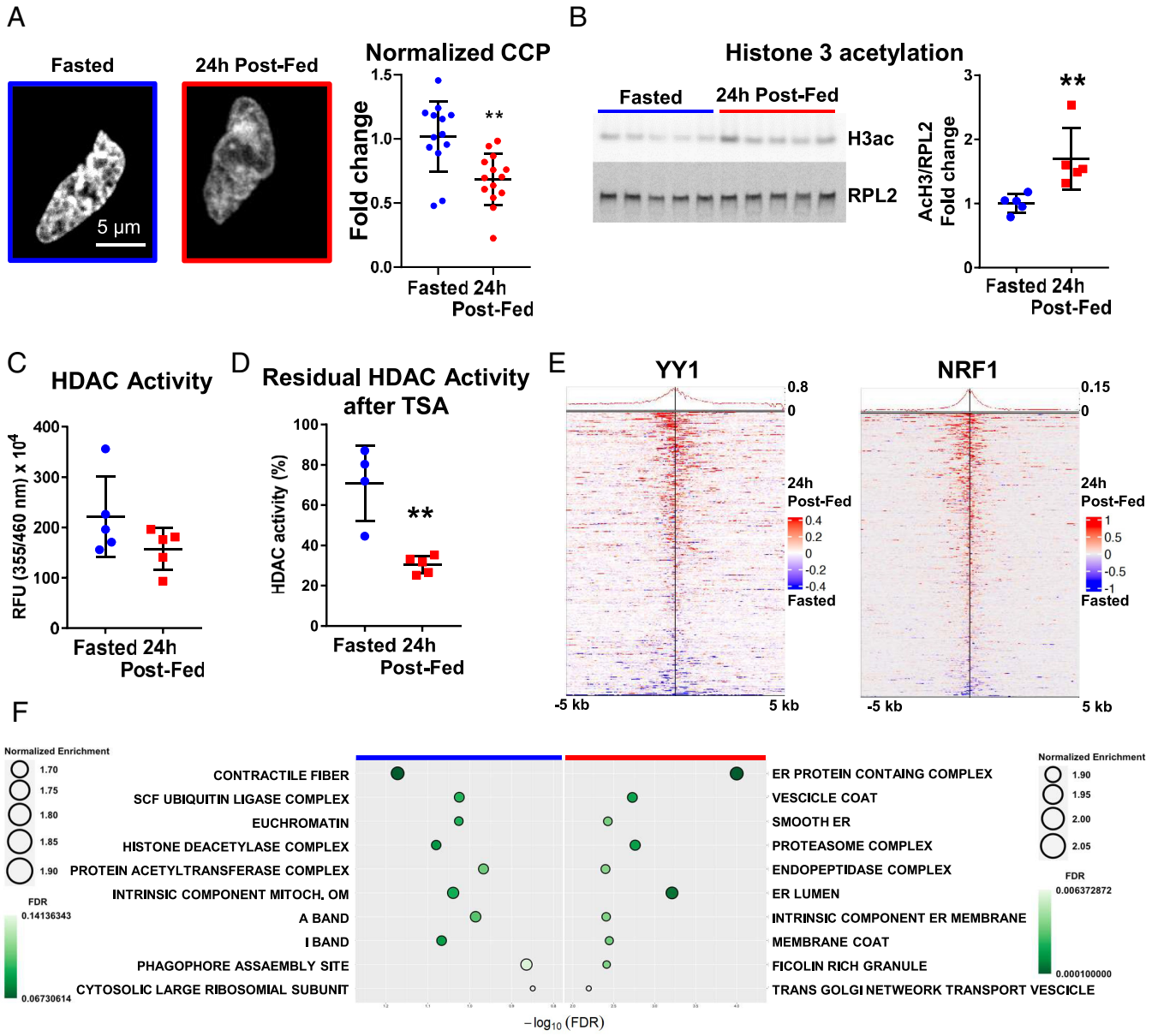

Fig. 4. ATACseq and RNAseq revealed changes in chromatin accessibility and gene-expression promoted by shifted HDAC activity. (*A*) DAPI stained nuclei of fasted (blue) and 24 h postfed (red) cardiomyocytes. CCP of fasted and 24 h postfed nuclei. Data from 13 fasted and 14 24 h postfed nuclei. Student *t* test applied. (*B*) Western blot of histone three acetylation. N = 5 hearts per group. Student *t* test applied. (*C*) HDAC activity assay without and (*D*) with TSA. N = 4 to 5 per group. Student *t* test applied. (*E*) Average ATAC-seq peak profile (*Top*) and signal heatmap (*Bottom*) for YY1 and NRF1. N = 3 per group. (*F*) GOCC enrichment analysis performed on genes that were down-regulated (blue) or up-regulated (red) in 24 h postfed hearts.

the endoplasmic reticulum compartment in 24 h postfed hearts (Fig. 4*F*), we hypothesized that cardiac metabolism was required to sustain protein homeostasis after feeding. Fasted and 24 h postfed hearts showed a distinct metabolomics profile (Fig. 5*A* and *SI Appendix*, Fig. S5), with 23 out of 118 compounds that were significantly different in concentration between the two groups (*SI Appendix*, Table S5). Quantitative enrichment analysis showed changes in the metabolism of many amino acids (Fig. 5*B*). Consistent with our hypothesis, protein folding was one of the top enriched gene ontology biological processes identified (Fig. 5*C* and *SI Appendix*, Fig. S7) and expression of the factor responsible for the enzymatic delivery of aminoacyl tRNAs to the ribosome, elongation factor eef1a, was increased (Fig. 5*D*). Metabolomics enrichment analysis showed increased metabolism of purines (Fig. 5*C*) supported by the ~eightfold increase of urate (*P*-value = 0.0054, *SI Appendix*, Table S5) and ~threefold increase of (S)(+)-allantoin (*P*-value = 0.0163, *SI Appendix*, Table S5), both products of the purine metabolic pathway. In agreement, we found that concentrations of most amino acids were increased or unchanged after feeding with the exceptions of L-aspartate (reduced by ~57%, *P*-value = 0.0355, *SI Appendix*, Table S5). This amino acid provides some of the nitrogen atoms to produce purine rings. We posited that increased purine metabolism was the result of increased needs of guanosine for the generation of guanosine triphosphate (GTP), the main source of energy in translation, and adenosine for generation of ATP. In fact, feeding increased the concentration of guanosine monophosphate (GMP) and adenosine monophosphate (AMP) and reduced the concentration of phosphocreatine (Fig. 5*E*), further suggesting increased energy demand in 24 h postfed python hearts as compared to fasted. In agreement with the increased concentration of AMP, the AMP-activated protein kinase (AMPK) was activated in 24 h postfed python hearts as compared to fasted hearts (Fig. 5*F*). This result is consistent with previous work in Burmese pythons (10, 29).

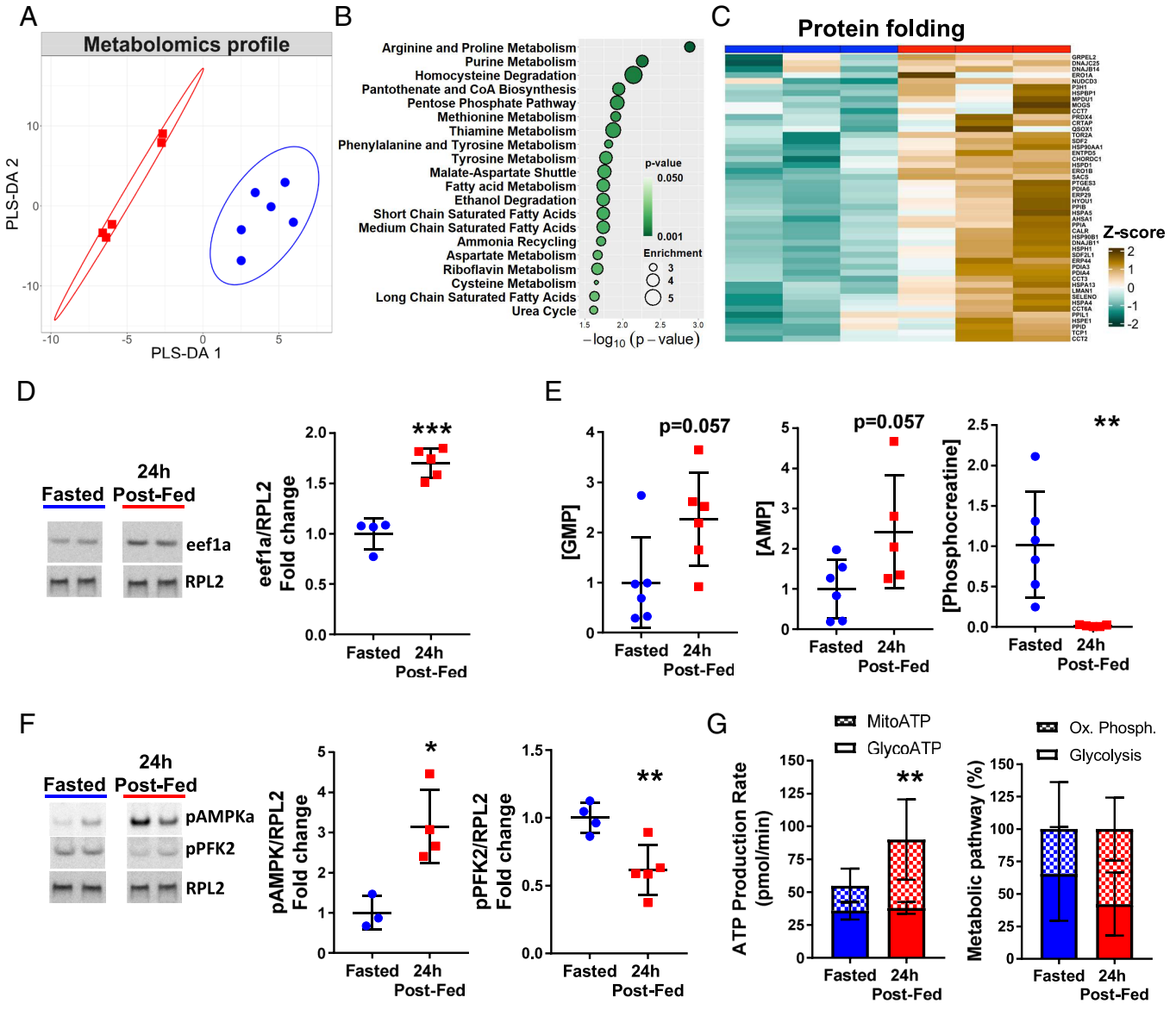

Fig. 5. Metabolic profiling reveals increased ATP production via oxidative phosphorylation and amino acid biosynthesis. (*A*) Partial least squares-discriminant analysis (PLS-DA) of fasted (blue) and 24 h postfed (red) metabolomics. (*B*) Enrichment analysis performed using compound concentrations. *P*-value < 0.05. (*C*) Heatmap of the expression of the core enrichment genes for the GOBP term "Protein folding." (*D*) Western blot and quantification of eeF1a in fasted (blue) and 24 h postfed (red) hearts. N = 4 to 5 per group. Student *t* test applied. (*E*) Normalized concentrations of GMP, AMP, and phosphocreatine detected in fasted (blue) and 24 h postfed (red) hearts via metabolomics. N = 5 to 6 hearts per group. (*F*) Western blot and quantification of phospho-AMPK and phospho-PFK2 in fasted (blue) and 24 h postfed (red) hearts. N = 3 to 5 per group. Student *t* test applied. (*G*) ATP production rate and percentage of metabolic pathway in fasted (blue) and 24 h postfed (red) isolated live cardiomyocytes measured with Seahorse. Two-way ANOVA with Sidak's multiple comparisons test between fasted and 24 h postfed and glycolytic ATP (GlycoATP) and mitochondria ATP (MitoATP). n = 8 wells and N = 3 animals per group.

AMPK is considered a master sensor and regulator of cellular energy that depends on the AMP/ADP:ATP ratio (30) and generally promotes fatty acid oxidation by phosphorylation and inhibition of acetyl-CoA carboxylase (ACC) and glycolysis by phosphorylation and activation of 6-phosphofructo-2-kinase (PFK2). We were unable to measure the phosphorylation site targeted by AMPK on PFK2 (Ser466 in humans) (31) but could measure another phosphorylation site (Ser483) that also activates glycolysis. However, in 24 h postfed ventricles, phosphorylation of PFK2 (Ser483) was reduced as compared to fasted hearts (Fig. 5*F*), suggesting that glycolysis may not be increased after feeding. To demonstrate what pathways were used for generating ATP in pythons, we measured ATP production rates in isolated cardiomyocytes using the Seahorse analyzer. In 24 h postfed python hearts, cardiomyocytes showed increased mitochondrial ATP production originating from oxidative phosphorylation, while glycolysis-derived ATP production rate did not change as compared to fasted cardiomyocytes (Fig. 5*G*). These results indicated that both energy production and energy demand were increased in postfed python hearts and that fatty acid β-oxidation was preferred over glycolysis as compared to fasted python hearts. We hypothesized that the increased energy requirements were essential to increase myofibril contraction and also to support protein turn-over and translation.

Discussion

Pythons are a unique animal model of extreme cardiac adaptation to feeding, but many aspects of their biology remain unknown. In this work, we integrated multiple approaches, including myofibril mechanics and multiomics tools, with the objective of identifying key regulatory pathways and molecular

mechanisms that underlie python cardiac adaptation to feeding. We confirmed that python hearts increased in mass 24 h after feeding (1, 9, 10). Both cardiac mass and cell size (fibers) increased by approximately 20% in 24 h postfed python hearts (Fig. 1 *B*–*E*). Sarcomere ultrastructure was also unchanged between fasted and 24 h postfed pythons (Fig. 1 *F*–*H*). Cardiac hypertrophy in pythons is not always observed after feeding (7, 32–35), and it is likely facultative and partly dependent on laboratory protocols related to maintenance feeding of the animals in the vivarium. Conflicting results may also emerge by the use of both ball and Burmese pythons (*python regius* and *python bivittatus*) in the literature. Both species respond similarly to feeding, but timing and extent of postprandial cardiac response might be different and merit further investigation, including later timepoints after feeding in ball pythons.

We sought to evaluate the activity of contractile proteins in isolation from other factors associated with excitation–contraction coupling. We used a fast solution switching technique to measure isometric force and contraction kinetics of myofibrils isolated from fasted and 24 h postfed python hearts. Isolated myofibrils showed increased maximal force generation after feeding (Fig. 1 *I* and *J*) but no change in the activation kinetics κ_{ACT} and κ_{TR} (*SI Appendix*, Fig. S1*B* and Fig. 1*K*), while the time of relaxation was increased most likely due to reduce rate of the slow, linear relaxation phase κ_{REL} (Fig. 1 *L* and *M*). Based on a 2-state cross-bridge model (36), the rate of force development (κ_{TR}) in myofibrils is equal to $f_{app} + g_{app}$, where f_{app} and g_{app} represent the apparent rate constants of the transition of the cross-bridges into the force-generating states and back into the nonforce generating states, respectively. The isometric linear κ_{REL} is equal to g_{app} (36, 37), which is also equal to the tension cost (isometric ATPase per unit force). Given that force is proportional to the apparent duty ratio [$f_{app}/(f_{app} + g_{app})$], the decrease in g_{app} in 24 h postfed myofibrils could explain the increase of maximal force, with no increase in energy cost per unit force. In other words, by slowing down the rate of cross-bridge detachment, the python heart increased force and avoided using more ATP per each given contraction. However, energy requirements would still increase because heart rates nearly doubled after feeding in ball pythons (2). Changes in active force generation and κ_{REL} could result also from changes in myosin isoform expression (38) or from phosphorylation of cardiac myosin binding protein-C (cMyBP-C) (39). Expression of myosin isoforms was similar between fasted and 24 h postfed hearts (*SI Appendix*, Fig. S1*D*). We confirmed that ball pythons expressed myosin 7b (14), a myosin with an atypical RNA expression pattern in mammals (no protein expressed in mammalian heart and major skeletal muscles) (40) that caused a sexually dimorphic dilated cardiomyopathy in mice when forcibly expressed (41). Both fasted and 24 h postfed myofibrils showed phosphorylation of cMyBP-C on Ser 309 (corresponding to Ser 304 in humans). The phosphorylation level was unchanged between the groups (*SI Appendix*, Fig. S1*E*). These results indicate that myofibril regulation in python cardiomyocytes may depend other mechanisms and further studies are needed. We then measured Ca^{2+} transients in isolated cardiomyocytes and found prolonged time-to-peak and Ca^{2+} decay after feeding (Fig. 2 *A* and *B*). Duration of Ca^{2+} transient can depend on a variety of mechanisms. We first tested whether increased myofibril Ca^{2+} sensitivity was the underlying cause for Ca^{2+} prolongation. Feeding did not change Ca^{2+} sensitivity of myofibrils (Fig. 2*C*) nor phosphorylation levels of PKA sites on cTnI (Ser 23/24 in human cTnI, *SI Appendix*, Fig. S2*F*), well-known targets of β-adrenergic signaling. Additionally, β-adrenergic signaling would accelerate Ca^{2+} transient rather than prolong it. These results support previous work showing that adrenergic tone is not particularly involved during digestion (2, 11). It is important to note that myofilament Ca^{2+} sensitivity is predominantly determined by the properties of the troponin–tropomyosin interaction (42), thus python thin filaments are likely not a target of postprandial cardiac adaptation. Another possible mechanism could be defective coupling of the sarcoplasmic reticulum. Similarly to lizards (17), python cardiomyocytes also lacked T-tubules (43) and presented a simplified sarcoplasmic reticulum with only peripheral couplings located below the sarcoplasm. After feeding, peripheral coupling length was increased (Fig. 2*D*) suggesting that Ca^{2+} release and reuptake was not defective at least structurally. A previous work suggested that the sodium–calcium exchanger (NCX) may play a more important role in Ca^{2+} cycling than the sarcoplasmic reticulum in ball pythons but that the sarcoplasmic reticulum may become important as contraction frequencies increase (44). In general, the small diameter of reptile cardiomyocytes compensates for the lack of internal Ca^{2+} releasing units. However, the space between myofibrils in 24 h postfed cardiomyocytes is increased as compared to fasted cells (Fig. 2*E*). Therefore, the increased volume that Ca^{2+} needed to travel would most likely cause a slowing down of the transients, proportionally to 1/V, where V is the volume. Other mechanisms could be contributing to the prolonged Ca^{2+} transients after feeding, such as posttranslational modifications or action potential prolongation. Other studies are needed to dissect the python excitation–contraction coupling.

We next aimed to measure the passive tension originating from the sarcomere specifically (45). Python myofibrils, both from fasted and 24 h postfed hearts, were more compliant (Fig. 3*A*) than mammalian myofibrils, as reported in the literature (18). Moreover, myofibrils further reduced their passive tension as a function of sarcomere length after feeding (Fig. 3*A* and *SI Appendix*, Fig. S3*A*). Because no change of isoform expression was identified (Fig. 3*B*), the reduced myofibril passive tension was likely due to posttranslational modifications on titin. As a result, cardiac tissue was less stiff after feeding (Fig. 3*C*), explaining the improved cardiac filling observed in python hearts after feeding (7) and supporting the postprandial elevation of cardiac output. As compared to mouse hearts (*SI Appendix*, Fig. S3*B*; mouse data previously published in ref. 21), python hearts were more than fourfold less stiff, despite indications that collagen content is higher (10). It may be of great interest to study collagen composition and assembly in python hearts.

Because tissue stiffness can affect epigenetics (46–48), we investigated chromatin accessibility and found increased open chromatin and histone three acetylation in 24 h postfed python hearts as compared to fasted (Fig. 4 *A* and *B*). Interestingly, feeding induced a specific reduction of sirtuin activity (Fig. 4 *C* and *D*), a family of histone deacetylases (HDAC Class III) (49). On the one hand, this result was unexpected as sirtuins are considered cardioprotective in the heart at many levels (50). On the other hand, it is well known that sirtuins are activated by caloric restriction (26), a state more likely existing in fasted python hearts. Further studies focused on the fasted state of pythons could help understand the role of sirtuins in this animal model. The total level of HDAC activity was not different between fasted and 24 h postfed ventricles, suggesting increased activity of other HDAC classes. We speculate that a coordinated change of activity in different HDAC classes may affect myofibril function, for instance, increased HDAC6 activity has been reported to reduce myofibril passive tension by deacetylating a lysine in the PEVK domain of titin (51).

Using high-resolution ATAC-seq, we found specific genomic regions that were more open and that enriched for motifs of the transcription factors YY1 and NRF1, suggesting that feeding had led to an increase in the activity of these transcription factors (Fig. 4*E*). YY1 is a ubiquitous and multifunctional zinc-finger transcription factor member of the Polycomb Group protein family, that is both a transcriptional activator and repressor (52). YY1 is important in cardiac development and inactivation of YY1 resulted in perinatal or embryonic death at E9 or E7.5, respectively (53). YY1 is also crucial for cardiomyocyte differentiation (54) and it is up-regulated in human heart failure, exerting a protective role via repression of αMyHC (55, 56). Notably, YY1 is a major regulator of metabolism, seemingly in a lineage-dependent manner. YY1 controls the metabolic program underlying both neural crest development and melanoma (57). In skeletal muscle, it promotes glycolysis and suppresses mitochondrial genes during stem cell activation (58) and, conversely, activates mitochondrial genes and oxidative phosphorylation during the differentiation stage (59). NRF1 has been recently associated with the regenerative potential of neonatal cardiomyocytes and protection from ischemia/reperfusion injury in mouse hearts via proteasome and antioxidant activity (28). The stress–response pathway activated by NRF2, another member of the vertebrate CNC transcription factor family, has been predicted to be activated in several tissues in Burmese pythons after feeding, but data were insufficient to determine activation in the heart (29).

We sought to link our ATAC-seq results with gene expression. The importance of gene expression and digestion has been previously investigated in Burmese pythons (13, 15, 16). Our main challenge was the lack of genome annotation for the ball python, but by increasing the sequencing depth, we were able to reliably identify genes using the latest Burmese python genome assembly (GCA_000186305.2). Gene ontology enrichment analysis pointed out differences in transcription, chromatin, and endoplasmic reticulum (Fig. 4*F*). Recently, gene expression was found to be significantly different between right and left sides of the ventricle in ball pythons (60), an observation that should be considered for future studies employing RNA-seq in pythons. In our dataset, 26% of significant differentially expressed genes (226 out of 840) were known targets of YY1 (117 were up-regulated and 109 downregulated) and 9% (77 out of 840) were targets of NRF1 (47 upregulated and 30 downregulated; *SI Appendix*, Table S4).

According to GO term annotation of the differentially expressed genes, cellular compartment and biological processes related to protein folding were enriched in python hearts after feeding (Fig. 4*F* and *SI Appendix*, Fig. S5), likely requiring a significant shift in metabolism. Our metabolomic profiling of fasted and 24 h postfed python hearts identified several differentially abundant metabolites (Fig. 5*A* and *SI Appendix*, Fig. S6 and Table S5), and enrichment analysis indicated striking changes in amino acid and purine metabolism (Fig. 5*B*). Accordingly, we found increased protein folding gene expression GO enrichment (Fig. 5*C* and *SI Appendix*, Fig. S7) and increased protein expression of the eukaryotic translation elongation factor 1A (eEF1A, Fig. 5*D*). Consistently, the concentration of GMP and AMP, products of GTP and ATP hydrolysis, was increased (Fig. 5*E*), while the concentration energy-rich phosphocreatine was significantly reduced. These results suggested that energy molecules were used to sustain the increased heart rate, cardiac output, and well as translation and protein folding. In fact, AMPK signaling was activated after feeding to promote further ATP production. Although we could not measure the phosphorylation site targeted by AMPK (and other kinases) on PFK2 (31), phosphorylation level of another important site for glycolysis activation was significantly reduced after feeding (Fig. 5*F*). This site is located in a recognition motif for several protein kinases, including PKA, once again supporting that β-adrenergic signaling is not involved in python postprandial adaptation. In Burmese python plasma, glucose concentration was unchanged after feeding (25), suggesting a relatively minor role for glycolysis in python postprandial cardiac adaptation. In contrast, triglycerides in python plasma increased more than 30 fold in 24 h after feeding (25) and likely represented the major fuel for heart response to feeding. To confirm this result, we measured ATP production in live cells and found the fatty acid oxidation was activated in python cardiomyocytes after feeding while glycolysis was unchanged (Fig. 5*G*). It has been suggested that the source of the energy comes from the meal despite it is only partly digested after 24 h. Burmese pythons show about 20% digestion of the meal when fed 25% of their body weight and this rate changes with meal size (61). Nonetheless, a previous work using enriched mice with the stable carbon isotope (^{13}C) demonstrated that pythons metabolized the meal to fuel the postprandial adaptation (62). Taken together, our results demonstrate that python hearts respond to feeding by using selected mechanisms that improve cardiac output while preserving energy and by increasing energy production.

Methods

A full description of experimental materials and methods is provided in *SI Appendix*, Methods.

Animals. Ball pythons (*python regius*) of both sexes were obtained as hatchlings from Bob Clark Reptiles and housed individually for 6 to 12 mo at ∼30 °C on a 10/14 h light/dark cycle. During this period, pythons were fed biweekly meals of intact rats until they grew to approximately 1,000 to 1,500 g. Before collection, pythons were acclimated to three 28-d feeding cycles. Meal-to-body mass ratio was used to quantify food content. After the last 28-d fast, pythons were fed rats ∼25% of their body mass. Pythons were sedated with isofluorane and then killed via decapitation either fasted or 24 h postfeeding. Tissue and plasma were collected, snap-frozen, and stored at −80 °C. All rats were housed in vivarium at ∼22 °C on a 10/14 h light/dark cycle. All procedures were conducted under the approval of the University of Colorado Boulder Institutional Animal Care and Use Committee.

Data, Materials, and Software Availability. The ATAC-seq and RNA-seq data are available through the Gene Expression Omnibus under the accession code GSE273555 (23) and GSE273554 (24), respectively. All study data are included in the article and/or *SI Appendix*.

ACKNOWLEDGMENTS. The fluorescence and Ca^{2+} imaging work was performed at the BioFrontiers Institute Advanced Light Microscopy Core (RRID: SCR_018302). Spinning disc confocal microscopy was performed on a Nikon Ti-E microscope supported by the BioFrontiers Institute and the Howard Hughes Medical Institute. We thank Dr. Monika Dzieciatkowska and Biological Mass Spectrometry Proteomics Core Facility at the University of Colorado School of Medicine for their mass spectrometry services. This research was supported by the Joyce and Dick Brown endowment to L.A.L. and C.C. was supported by a Human Frontiers Science Program fellowship (grant no. LT001449/2017-L) and American Heart Association postdoctoral fellowship (grant no. 20POST3521111).

Author affiliations: [a]Max Rubner Center for Cardiovascular Metabolic Renal Research (MRC), Deutsches Herzzentrum der Charité (DHZC), Charité University Medicine Berlin, Berlin 10115, Germany; [b]BioFrontiers Institute, University of Colorado Boulder, Boulder, CO 80303; [c]Department of Molecular, Cellular and Developmental Biology, University of Colorado Boulder, Boulder, CO 80303; [d]Division of Cardiology, Department of Medicine, University of Colorado Anschutz Medical Campus, Aurora, CO 80045; and [e]Department of Physiology and Biophysics, Anschutz Medical Campus, University of Colorado, Aurora, CO 80045

Author contributions: C.C., K.A., and L.A.L. designed research; C.C., K.C.W., C.D.O., S.P., J.C., C.J.W., and C.E.W. performed research; C.C., C.D.O., J.C., and M.A.A. contributed new reagents/analytic tools; C.C., K.C.W., C.D.O., S.P., J.C., and M.A.A. analyzed data; and C.C., C.D.O., M.A.A., and L.A.L. wrote the paper.

1. S. M. Secor, J. Diamond, A vertebrate model of extreme physiological regulation. *Nature* **395**, 659–662 (1998).
2. S. Enok, L. S. Simonsen, S. V. Pedersen, T. Wang, N. Skovgaard, Humoral regulation of heart rate during digestion in pythons (Python molurus and Python regius). *Am. J. Physiol. Regul. Integr. Comp. Physiol.* **302**, R1176–R1183 (2012).
3. S. M. Secor, J. Diamond, Adaptive responses to feeding in Burmese pythons: Pay before pumping. *J. Exp. Biol.* **198**, 1313–1325 (1995).
4. J. Overgaard, M. Busk, J. W. Hicks, F. B. Jensen, T. Wang, Respiratory consequences of feeding in the snake Python molorus. *Comp. Biochem. Physiol. A: Mol. Integr. Physiol.* **124**, 359–365 (1999).
5. S. M. Secor, S. E. White, Prioritizing blood flow: Cardiovascular performance in response to the competing demands of locomotion and digestion for the Burmese python, Python molurus. *J. Exp. Biol.* **213**, 78–88 (2010).
6. S. M. Secor, J. W. Hicks, A. F. Bennett, Ventilatory and cardiovascular responses of a python (Python molurus) to exercise and digestion. *J. Exp. Biol.* **203**, 2447–2454 (2000).
7. S. Enok *et al.*, Improved cardiac filling facilitates the postprandial elevation of stroke volume in Python regius. *J. Exp. Biol.* **219**, 3009–3018 (2016).
8. J. M. Starck, Functional morphology and patterns of blood flow in the heart of Python regius. *J. Morphol.* **270**, 673–687 (2009).
9. J. B. Andersen, B. C. Rourke, V. J. Caiozzo, A. F. Bennett, J. W. Hicks, Postprandial cardiac hypertrophy in pythons. *Nature* **434**, 37–38 (2005).
10. C. A. Riquelme *et al.*, Fatty acids identified in the Burmese python promote beneficial cardiac growth. *Science* **334**, 528–531 (2011).
11. T. Wang, E. W. Taylor, D. Andrade, A. S. Abe, Autonomic control of heart rate during forced activity and digestion in the snake Boa constrictor. *J. Exp. Biol.* **204**, 3553–3560 (2001).
12. N. Skovgaard, K. Møller, H. Gesser, T. Wang, Histamine induces postprandial tachycardia through a direct effect on cardiac H2-receptors in pythons. *Am. J. Physiol. Regul. Integr. Comp. Physiol.* **296**, R774–R785 (2009).
13. C. E. Wall *et al.*, Whole transcriptome analysis of the fasting and fed Burmese python heart: Insights into extreme physiological cardiac adaptation. *Physiol. Genomics* **43**, 69–76 (2011).
14. L. A. Lee *et al.*, Functional divergence of the sarcomeric myosin, MYH7b, supports species-specific biological roles. *J. Biol. Chem.* **299**, 102657 (2023).
15. J. Duan *et al.*, Transcriptome analysis of the response of Burmese python to digestion. *Gigascience* **6**, gix057 (2017).
16. T. A. Castoe *et al.*, The Burmese python genome reveals the molecular basis for extreme adaptation in snakes. *Proc. Natl. Acad. Sci. U.S.A.* **110**, 20645–20650 (2013).
17. S. Perni, V. R. Iyer, C. Franzini-Armstrong, Ultrastructure of cardiac muscle in reptiles and birds: Optimizing and/or reducing the probability of transmission between calcium release units. *J. Muscle Res. Cell Motil.* **33**, 145–152 (2012).
18. H. L. Granzier, T. C. Irving, Passive tension in cardiac muscle: Contribution of collagen, titin, microtubules, and intermediate filaments. *Biophys. J.* **68**, 1027–1044 (1995).
19. M. Gotthardt *et al.*, Cardiac splicing as a diagnostic and therapeutic target. *Nat. Rev. Cardiol.* **20**, 517–530 (2023), 10.1038/s41569-022-00828-0.
20. J. Perkin *et al.*, Phosphorylating Titin's cardiac N2B element by ERK2 or CaMKIIδ lowers the single molecule and cardiac muscle force. *Biophys. J.* **109**, 2592–2601 (2015).
21. C. Crocini, C. J. Walker, K. S. Anseth, L. A. Leinwand, Three-dimensional encapsulation of adult mouse cardiomyocytes in hydrogels with tunable stiffness. *Prog. Biophys. Mol. Biol.* **154**, 71–79 (2019), 10.1016/j.pbiomolbio.2019.04.008.
22. K. F. Tóth *et al.*, Trichostatin A-induced histone acetylation causes decondensation of interphase chromatin. *J. Cell Sci.* **117**, 4277–4287 (2004).
23. C. Crocini *et al.*, Data from "Post-prandial cardiac hypertrophy is sustained by mechanics, epigenetic, and metabolic reprogramming in pythons [ATAC-Seq]." GEO. https://www.ncbi.nlm.nih.gov/geo/query/acc.cgi?acc=GSE273555. Deposited 30 July 2024.
24. C. Crocini *et al.*, Data from "Post-prandial cardiac hypertrophy is sustained by mechanics, epigenetic, and metabolic reprogramming in pythons [RNA-Seq]." GEO. https://www.ncbi.nlm.nih.gov/geo/query/acc.cgi?acc=GSE273554. Deposited 30 July 2024.
25. J. A. Magida *et al.*, Burmese pythons exhibit a transient adaptation to nutrient overload that prevents liver damage. *J. Gen. Physiol.* **154**, e202113008 (2022).
26. L. Bordone, L. Guarente, Calorie restriction, SIRT1 and metabolism: Understanding longevity. *Nat. Rev. Mol. Cell Biol.* **6**, 298–305 (2005).
27. E. Kleiman, H. Jia, S. Loguercio, A. I. Su, A. J. Feeney, YY1 plays an essential role at all stages of B-cell differentiation. *Proc. Natl. Acad. Sci. U.S.A.* **113**, E3911–E3920 (2016).
28. M. Cui *et al.*, Nrf1 promotes heart regeneration and repair by regulating proteostasis and redox balance. *Nat. Commun.* **12**, 5270 (2021).
29. A. L. Andrew *et al.*, Growth and stress response mechanisms underlying post-feeding regenerative organ growth in the Burmese python. *BMC Genomics* **18**, 338 (2017).
30. S. Herzig, R. J. Shaw, AMPK: Guardian of metabolism and mitochondrial homeostasis. *Nat. Rev. Mol. Cell Biol.* **19**, 121–135 (2018).
31. A.-S. Marsin *et al.*, Phosphorylation and activation of heart PFK-2 by AMPK has a role in the stimulation of glycolysis during ischaemia. *Curr. Biol.* **10**, 1247–1255 (2000).
32. C. E. Slay, S. Enok, J. W. Hicks, T. Wang, Reduction of blood oxygen levels enhances postprandial cardiac hypertrophy in Burmese python (Python bivittatus). *J. Exp. Biol.* **217**, 1784–1789 (2014).
33. K. Hansen, P. B. M. Pedersen, M. Pedersen, T. Wang, Magnetic resonance imaging volumetry for noninvasive measures of phenotypic flexibility during digestion in Burmese pythons. *Physiol. Biochem. Zool.* **86**, 149–158 (2013).
34. P. S. Henriksen, S. Enok, J. Overgaard, T. Wang, Food composition influences metabolism, heart rate and organ growth during digestion in Python regius. *Comp. Biochem. Physiol. A: Mol. Integr. Physiol.* **183**, 36–44 (2015).
35. B. Jensen, C. K. Larsen, J. M. Nielsen, L. S. Simonsen, T. Wang, Change of cardiac function, but not form, in postprandial pythons. *Comp. Biochem. Physiol. A: Mol. Integr. Physiol.* **160**, 35–42 (2011).
36. B. Brenner, Effect of Ca2+ on cross-bridge turnover kinetics in skinned single rabbit psoas fibers: Implications for regulation of muscle contraction. *Proc. Natl. Acad. Sci. U.S.A.* **85**, 3265–3269 (1988).
37. C. Poggesi, C. Tesi, R. Stehle, Sarcomeric determinants of striated muscle relaxation kinetics. *Pflugers Arch.* **449**, 505–517 (2005).
38. I. Morano, C. Bletz, R. Wojciechowski, J. C. Rüegg, Modulation of crossbridge kinetics by myosin isoenzymes in skinned human heart fibers. *Circ. Res.* **68**, 614–618 (1991).
39. R. L. Moss, D. P. Fitzsimons, J. C. Ralphe, Cardiac MyBP-C regulates the rate and force of contraction in mammalian myocardium. *Circ. Res.* **116**, 183–192 (2015).
40. A. C. Rossi, C. Mammucari, C. Argentini, C. Reggiani, S. Schiaffino, Two novel/ancient myosins in mammalian skeletal muscles: MYH14/7b and MYH15 are expressed in extraocular muscles and muscle spindles. *J. Physiol.* **588**, 353–364 (2010).
41. A. K. Peter *et al.*, Expression of normally repressed myosin heavy chain 7b in the mammalian heart induces dilated cardiomyopathy. *J. Am. Heart Assoc.* **8**, e013318 (2019).
42. P. P. de Tombe *et al.*, Myofilament calcium sensitivity does not affect cross-bridge activation-relaxation kinetics. *Am. J. Physiol. Regul. Integr. Comp. Physiol.* **292**, R1129–R1136 (2007).
43. C. Ferrantini *et al.*, The transverse-axial tubular system of cardiomyocytes. *Cell Mol. Life Sci.* **70**, 4695–4710 (2013).
44. G. L. J. Galli, H. Gesser, E. W. Taylor, H. A. Shiels, T. Wang, The role of the sarcoplasmic reticulum in the generation of high heart rates and blood pressures in reptiles. *J. Exp. Biol.* **209**, 1956–1963 (2006).
45. W. A. Linke, V. I. Popov, G. H. Pollack, Passive and active tension in single cardiac myofibrils. *Biophys. J.* **67**, 782–792 (1994).
46. C. J. Walker *et al.*, Nuclear mechanosensing drives chromatin remodelling in persistently activated fibroblasts. *Nat. Biomed. Eng.* **5**, 1485–1499 (2021), 10.1038/s41551-021-00709-w.
47. T. L. Downing *et al.*, Biophysical regulation of epigenetic state and cell reprogramming. *Nat. Mater* **12**, 1154–1162 (2013).
48. C. J. Walker *et al.*, Extracellular matrix stiffness controls cardiac valve myofibroblast activation through epigenetic remodeling. *Bioeng. Transl. Med.* **7**, e10394 (2022).
49. S. Imai, C. M. Armstrong, M. Kaeberlein, L. Guarente, Transcriptional silencing and longevity protein Sir2 is an NAD-dependent histone deacetylase. *Nature* **403**, 795–800 (2000).
50. T. Finkel, C.-X. Deng, R. Mostoslavsky, Recent progress in the biology and physiology of sirtuins. *Nature* **460**, 587–591 (2009).
51. Y.-H. Lin *et al.*, HDAC6 modulates myofibril stiffness and diastolic function of the heart. *J. Clin. Invest.* **132**, e148333 (2022).
52. Y. Shi, E. Seto, L.-S. Chang, T. Shenk, Transcriptional repression by YY1, a human GLI-Krüippel-related protein, and relief of repression by adenovirus E1A protein. *Cell* **67**, 377–388 (1991).
53. I. Beketaev *et al.*, Critical role of YY1 in cardiac morphogenesis. *Dev. Dyn.* **244**, 669–680 (2015).
54. S. Gregoire *et al.*, Essential and unexpected role of Yin Yang 1 to promote mesodermal cardiac differentiation. *Circ. Res.* **112**, 900–910 (2013).
55. C. C. Sucharov *et al.*, The Ku protein complex interacts with YY1, is up-regulated in human heart failure, and represses α myosin heavy-chain gene expression. *Mol. Cell. Biol.* **24**, 8705–8715 (2004).
56. C. C. Sucharov, K. Dockstader, T. A. McKinsey, YY1 protects cardiac myocytes from pathologic hypertrophy by interacting with HDAC5. *Mol. Biol. Cell* **19**, 4141–4153 (2008).
57. S. Varum *et al.*, Yin Yang 1 orchestrates a metabolic program required for both neural crest development and melanoma formation. *Cell Stem Cell* **24**, 637–653.e9 (2019).
58. F. Chen *et al.*, YY1 regulates skeletal muscle regeneration through controlling metabolic reprogramming of satellite cells. *EMBO J.* **38**, e99727 (2019).
59. S. M. Blättler *et al.*, Defective mitochondrial morphology and bioenergetic function in mice lacking the transcription factor Yin Yang 1 in skeletal muscle. *Mol. Cell. Biol.* **32**, 3333–3346 (2012).
60. B. J. D. Boukens *et al.*, Catecholamines are key modulators of ventricular repolarization patterns in the ball python (Python regius). *J. Gen. Physiol.* **154**, e202012761 (2021).
61. S. M. Secor, J. Diamond, Effects of meal size on postprandial responses in juvenile Burmese pythons (Python molurus). *Am. J. Physiol. Regul. Integr. Comp. Physiol.* **272**, R902–R912 (1997).
62. J. M. Starck, P. Moser, R. A. Werner, P. Linke, Pythons metabolize prey to fuel the response to feeding. *Proc. R. Soc. Lond. B* **271**, 903–908 (2004).